Commun. Comput. Phys.
doi: 10.4208/cicp.150215.250515a

Vol. **18**, No. 5, pp. 1417-1444
November 2015

Piecewise Polynomial Mapping Method and Corresponding WENO Scheme with Improved Resolution

Qin Li[1,2,*], Pengxin Liu[1,2,*] and Hanxin Zhang[1,2]

[1] *State Key Laboratory of Aerodynamics, China Aerodynamic Research and Development Center, Mianyang, Sichuan, 621000, China.*
[2] *National Laboratory of Computational Fluid Dynamics, Beijing University of Aeronautics and Astronautics, Beijing, 100191, China.*

Communicated by Kun Xu

Received 15 February 2015; Accepted (in revised version) 25 May 2015

Abstract. The method of mapping function was first proposed by Henrick et al. [J. Comput. Phys. 207:542-547 (2005)] to adjust nonlinear weights in [0,1] for the fifth-order WENO scheme, and through which the requirement of convergence order is satisfied and the performance of the scheme is improved. Different from Henrick's method, a concept of piecewise polynomial function is proposed in this study and corresponding WENO schemes are obtained. The advantage of the new method is that the function can have a gentle profile at the location of the linear weight (or the mapped nonlinear weight can be close to its linear counterpart), and therefore is favorable for the resolution enhancement. Besides, the function also has the flexibility of quick convergence to identity mapping near two endpoints of [0,1], which is favorable for improved numerical stability. The fourth-, fifth- and sixth-order polynomial functions are constructed correspondingly with different emphasis on aforementioned flatness and convergence. Among them, the fifth-order version has the flattest profile. To check the performance of the methods, the 1-D Shu-Osher problem, the 2-D Riemann problem and the double Mach reflection are tested with the comparison of WENO-M, WENO-Z and WENO-NS. The proposed new methods show the best resolution for describing shear-layer instability of the Riemann problem, and they also indicate high resolution in computations of double Mach reflection, where only these proposed schemes successfully resolved the vortex-pairing phenomenon. Other investigations have shown that the single polynomial mapping function has no advantage over the proposed piecewise one, and it is of no evident benefit to use the proposed method for the symmetric fifth-order WENO. Overall, the fifth-order piecewise polynomial and corresponding WENO scheme are suggested for resolution improvement.

AMS subject classifications: 65M06, 65M12

Key words: WENO, mapping function.

*Corresponding author. *Email addresses:* `qin-li@vip.tom.com` (Q. Li), `liupengxin2008@163.com` (P. Liu)

1 Introduction

Following the introduction to the weighted essentially non-oscillatory (WENO) scheme [1], the subsequent efficient implementation [2] made the algorithm applicable to realistic problems. The weighting procedures and the smoothness indicator (IS) [2] eventually became a standard. After ten years of practices, WENO schemes especially the fifth-order version (WENO5) [2] have become one of the most popular high-order methods. Despite the success, some issues pertaining to WENO schemes were raised. It was Henrick et al. [3] who first pointed out that WENO5 failed to retain fifth-order accuracy at the critical point with $f_j'=0$. They further proposed the necessary and sufficient conditions for a scheme to obtain fifth-order accuracy. As a remedy, Henrick et al. [3] proposed a carefully designed mapping function, through which the difference between the nonlinear weight and its linear counterpart will usually have the order of Δx^3. The corresponding scheme was called WENO-M, which preserves fifth-order accuracy at the critical point [3].

The performance of WENO-M was tested by cases such as the 1-D Shu-Osher problem at 400 points [3] and the 2-D double Mach reflection problem [4]. The improvement on resolution was clearly shown through the comparison with WENO5. However, Borges et al. [5] argued the improvement was not due to enhancement of the convergence order, but came more from the ”assignment of larger weights to discontinuous stencils”. Still conforming to the accuracy requirement as in Ref. [3], they proposed a new IS by using a term comprised of higher order derivatives. The corresponding scheme was called as WENO-Z, and preliminary tests showed its slightly better performance than that of WENO-M [3,4].

Focusing on revising IS, Ha et al. [4] proposed a new algorithm by combining numerical approximations of first- and second-order derivatives. Two considerations were noticed in their work, i.e., an undivided difference for derivative discretization and a parameter to control ”the trade-off between the accuracies around the smooth region and discontinuity region”. The so-called WENO-NS scheme has shown better resolution in the computations of double-Mach reflection and 2-D Riemann problems when compared with WENO-M and WENO-Z.

Resolution enhancement may run the risk of numerical instability. Our tests showed that when using WENO-NS, the computation of a 2-D supersonic flow around half cylinder at $M=4$ blew up when the Steger-Warming scheme was used for flux splitting, to say nothing of tougher hypersonic cases. On the one hand, efforts continue on toward higher order and better resolution; on the other hand, schemes developed are expected to be robust and applicable for practical problems.

A procedure is proposed in this paper to improve resolution while preserving robustness. First, following the idea of mapping functions, specific piecewise polynomials of various orders are proposed, which are targeted toward resolution enhancement. The details are described in Section 2. Using the proposed methods, new fifth-order WENO schemes are obtained. Next, typical numerical tests are conducted in Section 3 with the comparison with WENO5, WENO-M, WENO-Z and WENO-NS. From computations of the 2-D Riemann problem, new schemes show improved resolution on shear-layer instability, while hypersonic computations indicate the schemes' capability for complex viscous/inviscid problems. In Section 4, the potential of using single polynomial as the mapping function is analyzed and the use of piecewise polynomial for symmetric WENO5 scheme is discussed. Finally, conclusions are drawn in Section 5.

2 Piecewise polynomial mapping method

In this section, we first review the accuracy analysis and the mapping function developed in Ref. [3]. Then we introduce the idea of piecewise polynomial mapping function in detail. Discussion is made on the relationship of resolution enhancement and the flat profile of the function at the location of the linear weight.

2.1 The review about the accuracy property, WENO-M [3], WENO-Z [5], and WENO-NS [4]

2.1.1 The accuracy requirement to preserve the fifth-order accuracy of WENO5

First, formulations of WENO5 are briefly reviewed. Consider the 1-D hyperbolic conservative law

$$u_t+f(u)_x=0. \tag{2.1}$$

Suppose the grids are equally partitioned as $x_j=j\Delta x$ where Δx denotes the interval and j is the index of the grid point, Eq. (2.1) at x_j can be re-written in conservative form as

$$(u_t)_j=-\left(\hat{f}_{j+1/2}-\hat{f}_{j-1/2}\right)\Big/\Delta x, \tag{2.2}$$

where $\hat{f}_{j+1/2}$ is the evaluation of $\hat{f}(x)$ at $x_{j+1/2}$, and $\hat{f}(x)$ is implicitly defined by $f(x)=\frac{1}{\Delta x}\int_{x-\Delta x/2}^{x+\Delta x/2}\hat{f}(x')dx'$. From Ref. [2], $\hat{f}(x)$ can be reconstructed through polynomials based on the value set of $\{f(x_j)\}$. To avoid entropy violation and improve stability, the flux $f(x_j)$ is usually split into f^+ and f^- according to the eigenvalue of $\partial f(u)/\partial u$. Taking positive splitting as an example and dropping the superscript '+' for brevity, the WENO scheme can be formulated as:

$$\hat{f}_{j+1/2}=\sum_{k=0}^{r'}\omega_k q_k^r, \tag{2.3}$$

where $r'=r-1$ for standard WENO and r denotes the grid point number of the basic stencil, ω_k is the nonlinear weight derived from the linear counterpart C_k^r, and q_k^r denotes the candidate scheme on basic stencils as $q_k^r=\sum_{l=0}^{r-1}a_{k,l}^r f\left(u_{j-r+k+l+1}\right)$. For WENO5 [2],

$r=3$, $C_k^3=\{0.3,0.6,0.1\}$, and coefficients $a_{k,l}^3$ can be found in Ref. [2]. For brevity, the superscript $'r'$ is dropped next. The derivation of ω_k is

$$\omega_k=\alpha_k\Big/\sum\nolimits_{l=0}^{2}\alpha_l, \tag{2.4}$$

where

$$\alpha_k=C_k\big/(\varepsilon+IS_k)^p \tag{2.5}$$

and usually $p=2$ and $\varepsilon=10^{-5}\sim 10^{-7}$ in Ref. [2]; IS_k denotes the smoothness indicator. Suppose the accuracy property of IS_k is

$$IS_k=D(1+\mathcal{O}(\Delta x^q)), \tag{2.6}$$

where D denotes certain factor and q represents some accurate order explained later, then [3]

$$\alpha_k=\frac{C_k}{D^p}(1+\mathcal{O}(\Delta x^q)), \tag{2.7}$$

$$\omega_k=C_k+\mathcal{O}(\Delta x^q). \tag{2.8}$$

In Ref. [2], IS of WENO5 (usually called as IS^{JS}) is defined as

$$IS_k^{JS}=\sum\nolimits_{l=1}^{2}\int_{x_{j-1/2}}^{x_{j+1/2}}\Delta x^{2l-1}\left(\partial^{(l)}q_k(x)\Big/\partial x^{(l)}\right)^2dx, \tag{2.9a}$$

or

$$\begin{cases} IS_0^{JS}=\frac{13}{12}\left(f_{j-2}-2f_{j-1}+f_j\right)^2+\frac{1}{4}\left(f_{j-2}-4f_{j-1}+3f_j\right)^2, \\ IS_1^{JS}=\frac{13}{12}\left(f_{j-1}-2f_j+f_{j+1}\right)^2+\frac{1}{4}\left(f_{j-1}-f_{j+1}\right)^2, \\ IS_2^{JS}=\frac{13}{12}\left(f_j-2f_{j+1}+f_{j+2}\right)^2+\frac{1}{4}\left(3f_j-4f_{j+1}+f_{j+2}\right)^2. \end{cases} \tag{2.9b}$$

For IS^{JS}, $D=(13/12)\left(f_j''\Delta x^2\right)^2$ and q will be 2 when $f_j'\neq 0$ [2] in Eq. (2.6). As mentioned in the introduction, Henrick et al. [3] first pointed out that at the critical point, $q=1$ and the fifth-order accuracy of WENO5 will not be retained. Further, Henrick et al. [3] proposed the following necessary and sufficient conditions for Eq. (2.3) at $r=3$ to retain the fifth-order:

$$\sum\nolimits_{l=0}^{2}(\omega_k-C_k)=\mathcal{O}\left(\Delta x^6\right), \tag{2.10a}$$

$$\left(3\omega_1{}^{j+1/2}-3\omega_1^{j-1/2}-\omega_2{}^{j+1/2}+\omega_2{}^{j-1/2}+\omega_3{}^{j+1/2}-\omega_3{}^{j-1/2}\right)=\mathcal{O}\left(\Delta x^3\right), \tag{2.10b}$$

$$\omega_k-C_k=\mathcal{O}\left(\Delta x^2\right). \tag{2.10c}$$

In Eq. (2.10b), the superscript $'j\pm1/2'$ represents the evaluation location of ω_k. For WENO5, Eq. (2.10a) is automatically satisfied, and so is Eq. (2.10c) when $f_j' \neq 0$. Under the same condition as $f_j' \neq 0$, Eq. (2.10b) holds according to Ref. [4,5] by symbolic calculation. Instead of the necessary and sufficient conditions of Eq. (2.10), a sufficient condition for accuracy retention is proposed as [3]

$$\omega_k - C_k = \mathcal{O}\left(\Delta x^3\right). \tag{2.11}$$

If Eq. (2.11) can be satisfied everywhere including the critical point, the accuracy can be well preserved theoretically. To fulfill this, Henrick at al. [3] carefully designed a mapping function to generate new ω_k from the original one of WENO5.

2.1.2 The mapping function and WENO-M

In Ref. [3], the concept of a mapping function (denoted by $g_k(\omega)$) was proposed for the aforementioned convergence order. The function is defined in [0,1] and satisfies

$$g_k(0)=0 \quad \text{and} \quad g_k(1)=1, \tag{2.12}$$

$$g_k(C_k)=C_k, \quad g_k^{(1)}(C_k)=0, \quad \text{and} \quad g_k^{(2)}(C_k)=0. \tag{2.13}$$

Let α_k in Eq. (2.5) re-computed as $\alpha_k(\omega_k)=g_k(\omega)$, then

$$\begin{aligned}\alpha_k(\omega_k) &= g_k(C_k)+{g_k}^{(1)}(C_k)(\omega_k-C_k)+\frac{{g_k}^{(2)}(C_k)}{2}(\omega_k-C_k)^2+\frac{{g_k}^{(3)}(C_k)}{6}(\omega_k-C_k)^3+\cdots \\ &= C_k+\mathcal{O}(\omega_k-C_k)^3,\end{aligned} \tag{2.14}$$

where ${g_k}^{(i)}(\omega)=\partial^i g_k(\omega)/\partial\omega^i$. As the last step, ω_k is updated by Eq. (2.4). It is easy to see Eq. (2.11) holds by using the revised ω_k. The concrete mapping function plays a key role in above algorithm. The one proposed by Henrick et al. [3] is:

$$g_k^H(\omega)=\frac{\omega\left(C_k+{C_k}^2-3C_k\omega+\omega^2\right)}{{C_k}^2+\omega(1-2C_k)}. \tag{2.15}$$

In short, after the original ω_k of WENO5 is modified by $\alpha_k(\omega)=g_k^H(\omega)$ and Eq. (2.4), a revised WENO5 will be obtained and referred as WENO-M [3].

2.1.3 WENO-Z [5] and WENO-NS [4]

In Section 3, results of WENO-Z [5] and WENO-NS [4] were used for comparison. For completeness, a brief introduction about the schemes are given as following. The analyses and more details of the schemes are suggested to Ref. [4,5].

Both schemes were designed under the framework of WENO by using Eqs. (2.1)-(2.5) but with new indicator of smoothness different from IS^{JS}. For WENO-Z, Borges et al. [5] proposed a new IS by introducing

$$\tau_5=\left|IS_0^{JS}-IS_2^{JS}\right|. \tag{2.16}$$

Then the new indicator IS^z and α_k^z are defined as

$$IS_k^z = \left(\frac{IS_k^{JS} + \varepsilon}{IS_k^{JS} + \tau_5 + \varepsilon} \right), \tag{2.17}$$

$$\alpha_k^z = \frac{C_k}{IS_k^z}, \tag{2.18}$$

where usually $\varepsilon = 10^{-40}$. Furthermore, a concrete form of α_k^z was proposed in Ref. [5] as $\alpha_k^z = C_k\big(1 + (\tau_5/(IS_k^{JS} + \varepsilon))^q\big)$. Regarding to the value of q, Borges et al. [5] pointed out, "to recover the fifth-order accuracy at a first-order critical point" of the scheme, $q=2$, which is the choice in this paper thereby.

By using the revised α_k^z as α_k in Eq. (2.4), the final ω_k is obtained and the algorithm of WENO-Z is fulfilled. For implementations of WENO-NS, Ha et al. [4] first introduced another IS as

$$IS_k^{NS} = \xi \big| (1-k) f_{j-2+k} + (2k-3) f_{j-1+k} + (2-k) f_{j+k} \big| + \big| f_{j-2+k} - 2 f_{j-1+k} + 3 f_{j+k} \big|, \tag{2.19}$$

where ζ is a coefficient with the value 0.4 in Ref. [4]. Next let

$$\alpha_k^{NS} = C_k \left(1 + \frac{\zeta}{\left(\varepsilon + IS_k^{NS}\right)^2} \right), \tag{2.20}$$

where $\zeta = \frac{1}{2}\left(|IS_0 - IS_2|^2 + g^{NS}\left(|f_{j+1} - f_j|\right)^2 \right)$, $g^{NS}(x) = \frac{x^3}{1+x^3}$, and usually $\varepsilon = 10^{-40}$. At last, using α_k^{NS} as α_k in Eq. (2.4), the algorithm of WENO-NS is finished.

2.2 Piecewise polynomial mapping function and the mapped WENO scheme

In Ref. [3], WENO-M has shown its resolution enhancement by numerical examples. It is a natural thought to check if there are other functions which have better numerical resolutions.

Before making further analysis, it is necessary to discuss the properties a mapping function should have. From Eqs. (2.10)-(2.11) and the view of Borges et al. [5], one of the understanding is that ω_k should approach C_k as close as possible provided the computation is stable. The mathematical interpretation of the understanding is that at the location $\omega = C_k$, the mapping function should have a distribution close to $g_k(\omega) = C_k$ or have a flat profile. It is conceivable that when the function is flatter at $\omega = C_k$, the final value of ω will be closer to C_k, and the corresponding nonlinear scheme will be more like its linear counterpart. Usually, such a situation is in favor of resolving subtle structures such as shear-layer instabilities and vortices in turbulence.

Besides the concerns above, other restrictions exist, e.g., Eqs. (2.12) and (2.13). In short, the property requirements can be summarized as:

1. Boundary conditions. This restriction has been described by Eq. (2.12), which makes the scheme behave like WENO5 when discontinuities are met. Considering the fact that $g_k(\omega)=\omega$ is just WENO5, the emphasis on the numerical stability implies that the profile of mapping function should quickly converge towards $g_k(\omega)=\omega$ near the endpoints of $[0,1]$.
2. Accuracy. This property has been described by Eq. (2.13).
3. Monotonicity. Because the nonlinear weights reflect the smoothness of the solution, the stencil with unsmooth solution should have less contribution to the derivation of $\hat{f}_{j+1/2}$. Therefore, the mapping function should not change the order of original weights. This implies the monotonicity should be preserved.
4. The flat profile of the mapping function at $\omega=C_k$. As suggested by Borges et al. [5], "assignment of larger weights to discontinuous stencils" is favorable for the resolution of the scheme. This statement implies that the nonlinear weight should be close to its linear counterpart whenever possible, or the distribution of the mapping function should be close to the horizontal line at $\omega=C_k$. As discussed in the beginning of this section, the flatness of the function is favorable for the resolution of the scheme providing the computation is stable.
5. The "nice" appearance, namely, the function has a distribution lying above $g_k(\omega)=\omega$ at $[0,C_k]$ and underneath it at $[C_k,1]$. A monotone polynomial might still oscillate around $g_k(\omega)=\omega$ and violate this property thereby. Taking the interval $[C_k,1]$ as an example and supposing properties (1)-(3) are satisfied, the function locally lying above $g_k(\omega)=\omega$ will have a value more far away from $g_k(\omega)=C_k$ than that of the one lying underneath it. This property is an optional one and is well preserved by g_k^H [3].

Regarding properties (1) and (4), the following relations can be devised as their mathematical interpretations respectively

$$g_k{}^{(1)}(0,1)=1, \quad g_k{}^{(i)}(0,1)=0 \quad \text{for } i\geq 2, \tag{2.21}$$

$$g_k{}^{(i)}(C_k)=0 \quad \text{for } i\geq 3, \tag{2.22}$$

where Eq. (2.21) corresponds to the part of property (1) except Eq. (2.12).

According to previous discussions, in order to improve resolution it is vital to make the nonlinear weights ω be close to linear counterparts C_k as much as possible while they are still eligible for stable shock capturing. Among the properties, item (4) should be most correlated to the issue. For realizing the property, the mapping function g_k^H is one of the choices, and it is worth to seek other functions through which ω can be more close to C_k for stable computations with shocks. Firstly it is a natural thought to use polynomials with various orders as candidates for mapping functions. But after testing, it is hard to find qualified polynomials which efficiently satisfy all five properties for all C_k of WENO5. Some practices will be shown in Section 4. The solution to this plight is the understanding that it is actually unnecessary to use the single function defined in [0,1] to satisfy Eqs. (2.12)-(2.13) and (2.21)-(2.22). By using piecewise polynomials which are separately defined at $[0,C_k]$ and $[C_k,1]$, all properties can be easily reached. If the left and right piecewise functions are denoted as g_k^L and g_k^R, the derivation conditions are proposed as follows:

For g_k^L,

$$g_k{}^L(0)=0,\ \text{optionally}\ \left(g_k{}^L\right)^{(1)}(0^+)=1\ \text{and}\ \left(g_k{}^L\right)^{(i)}(0^+)=0\ \text{for}\ i\geq 2, \tag{2.23a}$$

$$g^L{}_k(C_k)=C_k,\quad g^{L(i)}_{\ k}(C_k{}^-)=0\ \text{for}\ i=1,2\ \text{and optionally for}\ i\geq 3. \tag{2.23b}$$

For g_k^R,

$$g_k{}^R(1)=1,\ \text{optionally}\ \left(g_k{}^R\right)^{(1)}(1^-)=1\ \text{and}\ \left(g_k{}^R\right)^{(i)}(1^-)=0\ \text{for}\ i\geq 2, \tag{2.24a}$$

$$g^R{}_k(C_k)=C_k,\quad g^{R(i)}_{\ k}(C_k{}^+)=0\ \text{for}\ i=1,2\ \text{and optionally for}\ i\geq 3, \tag{2.24b}$$

where ”optionally” means conditions after it is realized on a case-by-case basis.

It is well-known that a third-order polynomial can be established if necessary parts in Eq. (2.23) or (2.24) are satisfied. A simple check on the polynomial will show that no improvement on the property (4) is achieved compared with $g_k^H(\omega)$. By raising the order of the polynomial, free parameters appear which can be used to improve properties. Take g_k^L as an example, property (1) can be improved by optional parts in Eq. (2.23a) and so does property (4) by optional parts in Eq. (2.23b). What is more, the two properties can be emphasized unevenly, which is accomplished by realizing more or less optional conditions in Eqs. (2.23a) and (2.23b). A similar process can be done for g_k^R. After trying possible combinations, three polynomials with orders 4-6 are chosen. The choices of the optional conditions in Eqs. (2.23)-(2.24) are shown in Table 1.

Table 1: The choices of optional conditions.

Order	$g_k{}^L$	$g_k{}^R$	Remarks
4	$(g_k{}^L)^{(3)}(C_k{}^-)=0$	$(g_k{}^R)^{(3)}(C_k{}^+)=0$	Enforce the property (4)
5	$(g_k{}^L)^{(3,4)}(C_k{}^-)=0$	$(g_k{}^R)^{(3,4)}(C_k{}^+)=0$	Enforce the property (4)
6	$(g_k{}^L)^{(1)}(0^+)=1$ $(g_k{}^L)^{(3,4)}(C_k{}^-)=0$	$(g_k{}^R)^{(1)}(1^-)=1$ $(g_k{}^R)^{(3,4)}(C_k{}^+)=0$	Enforce both the property (1) and (4)

Letting $a=\omega/C_k$ and $b=1/(C_k-1)$, the obtained functions can be summarized in Table 2 after properly rearranging terms. The three piecewise functions are abbreviated together as PPM or PPM*n* in this study, where n denotes the order of the polynomial.

Compared with $g_k^H(\omega)$, piecewise polynomials in the section $[0,C_k]$ are shown in Fig. 1 and those in the section $[C_k,1]$ are shown in Fig. 2. From the figures, it can be shown that:

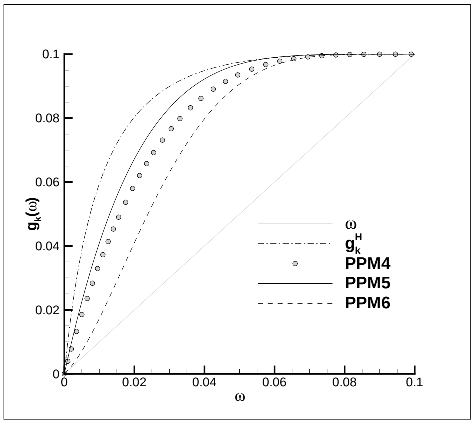

(a) $C_k = 0.1$

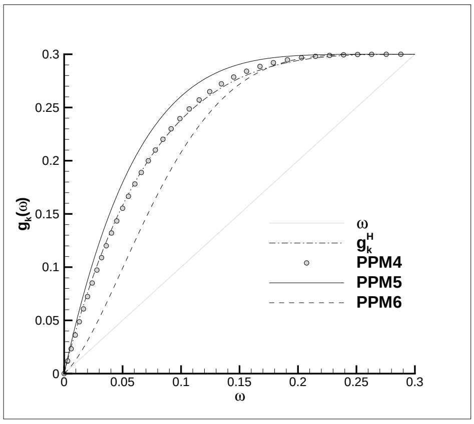

(b) $C_k = 0.3$

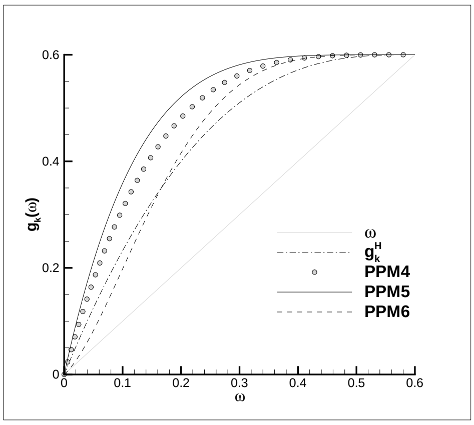

(c) $C_k = 0.6$

Figure 1: Distributions of PPM at $[0,C_k]$.

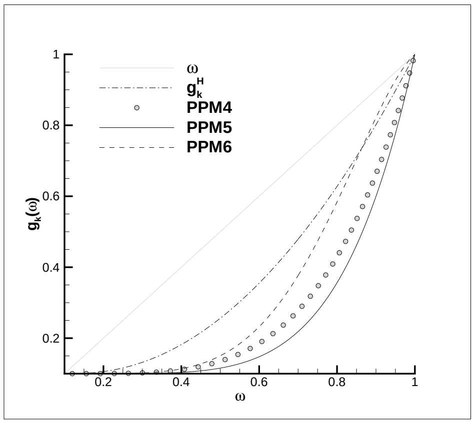

(a) $C_k = 0.1$

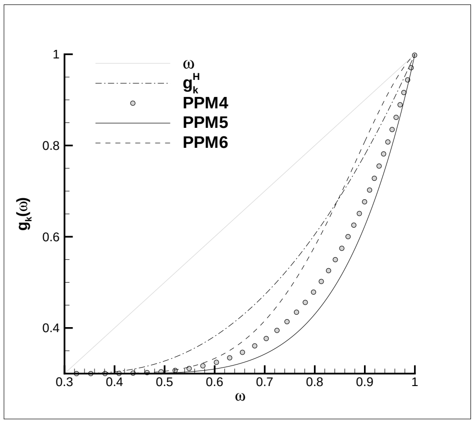

(b) $C_k = 0.3$

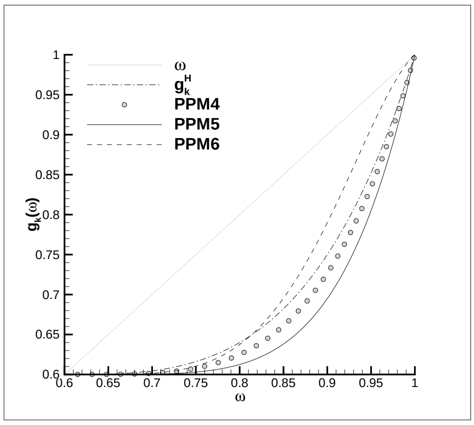

(c) $C_k = 0.6$

Figure 2: Distributions of PPM at $[C_k,1]$.

Table 2: The piecewise polynomial mapping functions.

Order	The mapping function
4	${g_k}^L$: $C_k\left[1-(a-1)^4\right]$, ${g_k}^R$: $C_k-b^3(\omega-C_k)^4$
5	${g_k}^L$: $C_k\left[1+(a-1)^5\right]$, ${g_k}^R$: $C_k+b^4(\omega-C_k)^5$
6	${g_k}^L$: $\omega\left(1+10a-30a^2+35a^3-19a^4+4a^5\right)$ ${g_k}^R$: $b^5\left[\begin{array}{l}\left(10{C_k}^4-10{C_k}^3+5{C_k}^2-C_k\right)+\left({C_k}^5-25{C_k}^4\right)\omega+\left(10{C_k}^4+50{C_k}^3\right)\omega^2\\-\left(30{C_k}^3+50{C_k}^2\right)\omega^3+\left(35{C_k}^2+25C_k\right)\omega^4-(19C_k+5)\omega^5+4\omega^6\end{array}\right]$

1. All PPM functions distribute more flatly at C_k than $g_k^H(\omega)$, or the revised ω will be more close to C_k when the original ω has a value close to C_k. This indicates that the aforementioned motivation is realized.

2. PPM5 distributes most flatly at C_k and encloses other functions by itself and $g_k(\omega)=\omega$ at nearly all cases except $C_k=0.1$. The distribution indicates the corresponding nonlinear weights will be relatively closer to C_k and therefore is potentially favorable for resolution improvement.

3. PPM6 shows a flatter distribution at C_k when compared with $g_k^H(\omega)$ and the quickest convergence to $g_k(\omega)=\omega$ at the two endpoints of $[0,1]$, which implies an emphasis on stability while still concerning the resolution.

4. PPM4 falls in an intermediate position between PPM5 and PPM6.

Using similar procedures as WENO-M [3], i.e., re-computing ω_k by Eq. (2.4) after redefining $\alpha_k=$PPM(ω_k), a new fifth-order WENO scheme can be obtained. According to the order of PPM, the corresponding schemes are called as WENO-PPM4, WENO-PPM5, and WENO-PPM6 respectively.

In the next sections, typical numerical examples are used to show the performance of WENO-PPM*n* schemes and comparisons among themselves. In addition, results of WENO-PPM*n* are compared to that of WENO5, WENO-M, WENO-Z and WENO-NS. In Eq. (2.5) of above schemes, $\varepsilon=10^{-40}$ except $\varepsilon=10^{-16}$ for WENO5.

2.3 The property of the convergence order

Following the commonly used way [3–5], the linear advection problem with smooth and discontinuous initial distributions is chosen to show the convergence order of WENO-

PPM5. The linear advection equation is

$$u_t + u_x = 0,$$

where $x \in [-1,1]$. Standard fourth-order Runge-Kutta scheme was used to discretize the temporal term, and the time step is chosen as $(\Delta x)^{5/4}$ to minimize the influence of temporal errors. The value of ε in various schemes has been given in previous section.

(1) The smooth initial distribution case

The initial condition is

$$u(x,t=0) = \sin\left(\pi x - \frac{\sin(\pi x)}{\pi}\right).$$

The computation is advanced to $t=2$. In Table 3, numerical errors and corresponding orders are shown with the comparison of various schemes, namely, WENO5, WENO-M, WENO-Z, WENO-NS, and WENO5 using ideal linear weights. In the table, "N" denotes the grid number.

Table 3: Convergence properties of various schemes with the smooth initial condition.

N	WENO5		WENO-M		WENO-Z	
	L_2 (order)	L_∞ (order)	L_2 (order)	L_∞ (order)	L_2 (order)	L_∞ (order)
10	7.36e-2(- -)	1.36e-1(- -)	4.54e-2(- -)	9.00e-2(- -)	3.37e-2(- -)	5.79e-2(- -)
20	6.07e-3(3.60)	1.41e-2(3.27)	2.41e-3(4.24)	5.61e-3(4.00)	1.92e-3(4.13)	4.10e-3(3.82)
40	4.77e-4(3.67)	1.10e-3(3.68)	9.58e-5(4.65)	2.12e-4(4.73)	9.35e-5(4.36)	2.26e-4(4.18)
80	2.56e-5(4.22)	8.85e-5(3.64)	3.07e-6(4.96)	6.69e-6(4.98)	3.06e-6(4.93)	6.69e-6(5.08)
160	1.62e-6(3.98)	8.15e-6(3.44)	9.66e-8(4.99)	2.10e-7(4.99)	9.66e-8(4.99)	2.10e-7(4.99)
320	1.19e-7(3.76)	8.27e-7(3.30)	3.02e-9(5.00)	6.55e-9(5.00)	3.02e-9(5.00)	6.55e-9(5.00)
640	9.19e-9(3.69)	8.64e-8(3.26)	9.43e-11(5.00)	2.05e-10(5.00)	9.43e-11(5.00)	2.05e-10(5.00)
	WENO-NS		WENO-PPM5		Ideal weights	
10	4.59e-2(- -)	8.94e-2(- -)	5.34e-2(- -)	1.01e-1(- -)	4.96e-2(- -)	9.03e-2(- -)
20	2.84e-3(4.01)	6.24e-3(3.84)	3.00e-3(4.15)	5.98e-3(4.07)	2.89e-3(4.10)	5.98e-3(3.92)
40	9.76e-5(4.86)	2.07e-4(4.91)	9.93e-5(4.91)	2.11e-4(4.82)	9.80e-5(4.88)	2.12e-4(4.82)
80	3.08e-6(4.99)	6.68e-6(4.95)	3.08e-6(5.01)	6.69e-6(4.98)	3.08e-6(4.99)	6.69e-6(4.99)
160	9.67e-8(4.99)	2.10e-7(4.99)	9.67e-8(4.99)	2.10e-7(4.99)	9.67e-8(4.99)	2.10e-7(4.99)
320	3.02e-9(5.00)	6.55e-9(5.00)	3.02e-9(5.00)	6.55e-9(5.00)	3.01e-9(5.01)	6.55e-9(5.00)
640	9.43e-11(5.00)	2.05e-10(5.00)	9.43e-11(5.00)	2.05e-10(5.00)	9.43e-11(5.00)	2.05e-10(5.00)

Unsurprisingly, WENO-PPM5 has gained the fifth-order convergence like its counterparts except WENO5. Carefully comparing the L_∞ order of nonlinear schemes with that of the linear one, it can be found that the order of WENO-PPM5 is the closest to that of the linear scheme on the intermediate grid number 40 and 80.

(2) The discontinuous initial distribution case

The initial condition is

$$u_0(x)=\begin{cases} -\sin(\pi x)-\frac{1}{2}x^3, & \text{if } -1\leq x<0, \\ -\sin(\pi x)-\frac{1}{2}x^3+1, & \text{if } 0\leq x\leq 1. \end{cases}$$

The computation was conducted with $\Delta x=0.01$ and run to $t=2$. Fig. 3 shows the result of WENO-PPM5 with the comparison with WENO5, WENO-M, WENO-Z and WENO-NS. Generally, various schemes behave similarly at the smooth region, while WENO-PPM5 shows a slightly sharper distribution at the discontinuity.

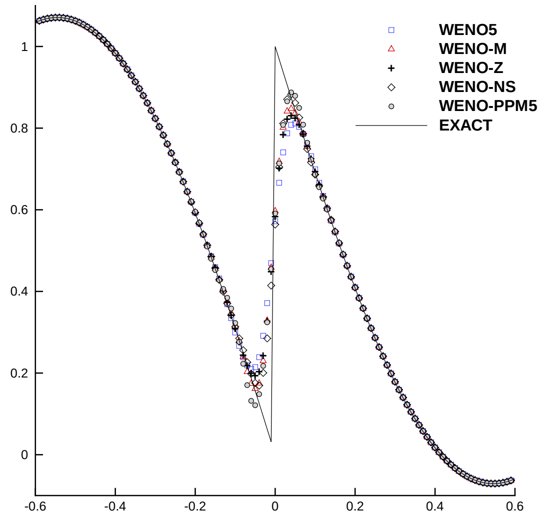

Figure 3: Numerical solutions of the linear advection equation with discontinuous initial condition.

In more detail, nonlinear weights are shown in Fig. 4 together with the linear ones. All weights have small values around the discontinuity $(x\approx 0)$ but with different quantity levels for different schemes. In addition, WENO5 has the smallest values at $x\approx 0$ while WENO-NS has the largest ones. But as said before, too large weights near the discontinuity implies the risk of numerical instability, which might make computations blow up at practical supersonic problems.

3 Numerical tests

Typical 1-D and 2-D problems are used to test the piecewise polynomial mapping method. In all cases, Steger-Warming splitting, characteristic projection and characteristic variables were adopted. As regard to the temporal algorithm, the third-order TVD Runge-

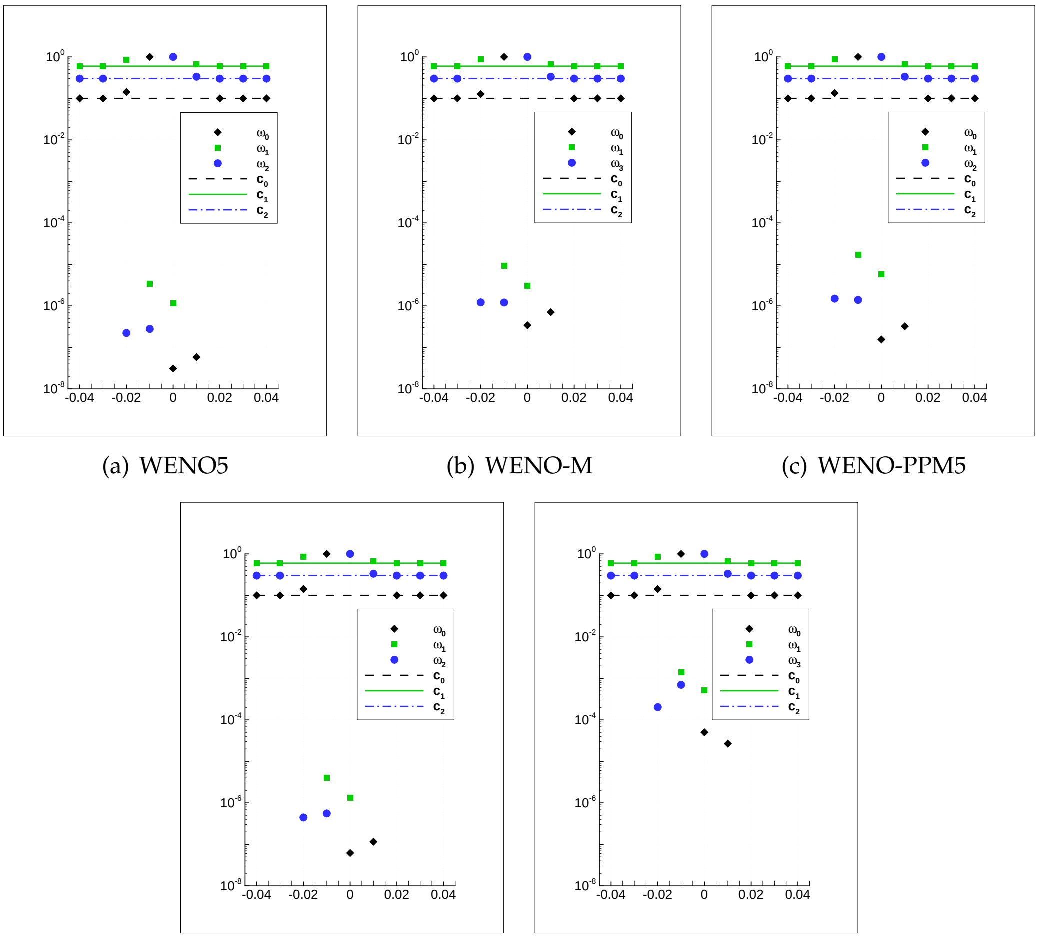

(a) WENO5 (b) WENO-M (c) WENO-PPM5

(d) WENO-Z (e) WENO-NS

Figure 4: The distribution of the ideal weights C_k and weights ω_k of various schemes.

Kutta scheme was used for unsteady problems in case (1)-(3) and (5), and LU-SGS was used for the steady one in case (4).

(1) Shu-Osher problem

The range of x is $[-5,5]$ and the initial conditions about the density, velocity and pressure are

$$(\rho,u,p)=\begin{cases} (3,857143,2.629369,10.3333), & x<-4, \\ (1+0.2\sin(5x),0,1), & x\geq -4. \end{cases}$$

The computation is conducted using 200 uniform grid points and runs up to $t=1.8$ with $\Delta t=0.003$. The comparison of three WENO-PPMn schemes is shown in Fig. 5, where the result of WENO5 on 1600 grids is referenced as the "exact" solution. Relatively speaking, WENO-PPM5, which is with particular emphasis on resolution (see Table 1 and

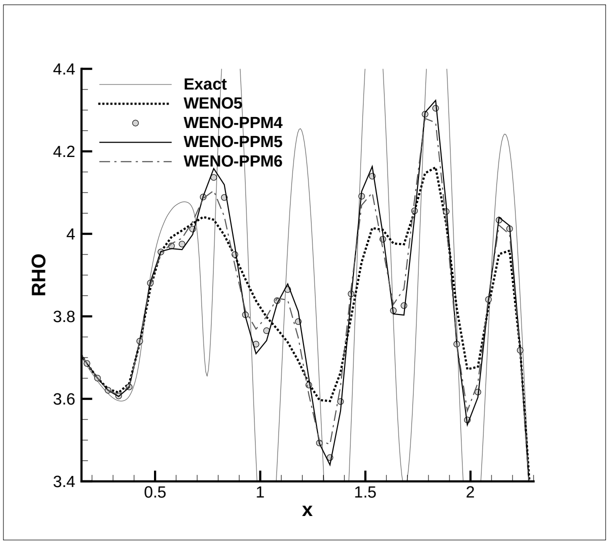

Figure 5: The comparison on density distribution of WENO-PPMn schemes.

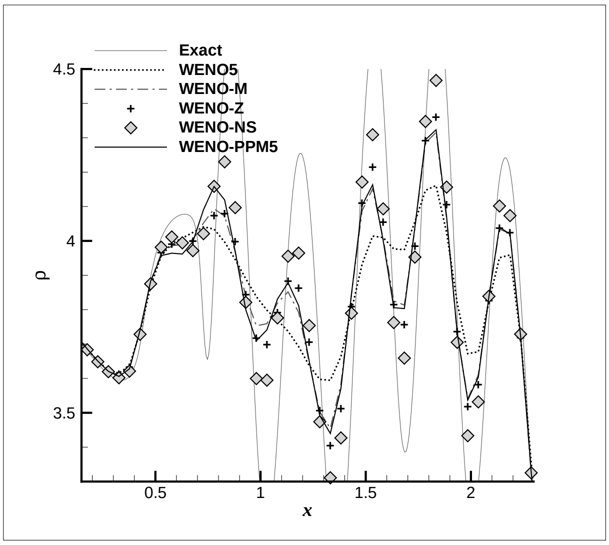

Figure 6: The comparison on density distribution of various WENO type schemes.

Figs. 1-2), shows the best description of the density oscillations. WENO-PPM6, which has more consideration on the stability, shows the least resolution; while the performance of WENO-PPM4 is very close to that of WENO-PPM5.

Next, comparisons are made among WENO5, WENO-M, WENO-Z, WENO-NS, and WENO-PPM5 in Fig. 6. WENO-PPM5 shows better performance than WENO-M at the region [0.7,1.2] while compared with WENO-Z, the scheme first shows a slightly better resolution at around $x=0.8$ but becomes relatively less resolved after $x \approx 1$. Consistent with Ref. [4], WENO-NS shows the best resolution. Although the performance of WENO-PPMn schemes is not the best in this case, the best one WENO-NS fails to pass the subsequent test of double-Mach reflection when Steger-Warming flux splitting is used. As it will be seen, WENO-PPMn show improved resolution in 2-D computations, where new mapping functions are thought to make nonlinear weights to be more close to their linear counterparts.

(2) Riemann problem

In Ref. [6], a series of 2-D Riemann problems was proposed to check the performance of positive schemes, which later became favorable cases to test the resolution of numerical methods [7]. Configuration 13 in Ref. [6], which is sketched in Fig. 7, is chosen here for testing. The initial conditions of the case are:

$$\begin{aligned}
&\text{Zone 1: } \rho_1=1,\ p_1=1,\ u_1=0,\ v_1=-0.3;\\
&\text{Zone 2: } \rho_2=2,\ p_2=1,\ u_2=0,\ v_2=0.3;\\
&\text{Zone 3: } \rho_3=1.0625,\ p_3=0.4,\ u_3=0,\ v_3=0.8145;\\
&\text{Zone 4: } \rho_4=0.5313,\ p_4=0.4,\ u_4=0,\ v_4=0.4276.
\end{aligned}$$

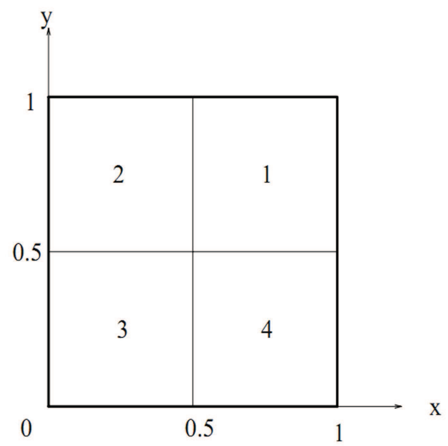

Figure 7: The schematic of Riemann problem.

The Euler equation is solved on 1200×1200 grids, and the computations proceed to $t=0.3$ at $\Delta t=0.00015$. The investigation in this case is focused on the description of instability of the slip line, which is indicated by a box in Fig. 8. The following schemes were tested: WENO5, WENO-M, WENO-Z, WENO-NS, and WENO-PPM4 to WENO-PPM6. In addition, the results of WENO7 and a hybrid compact/WENO scheme from Ref. [7] are directly cited here for comparison. The results are shown in Figs. 8-14 except those of WENO5 and WENO-Z. Results of these two latter schemes were very similar to that of WENO-M and are omitted. From the figures, the following can be observed. WENO-M

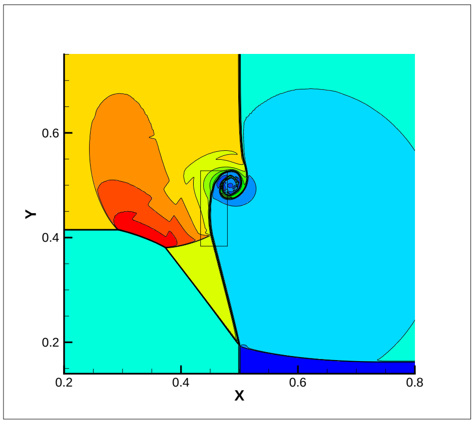

Figure 8: The density contour of WENO-M.

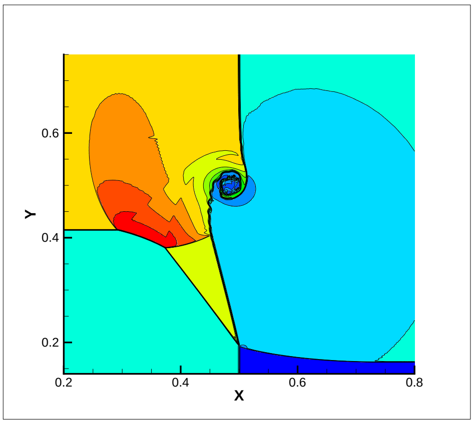

Figure 9: The density contour of WENO-NS.

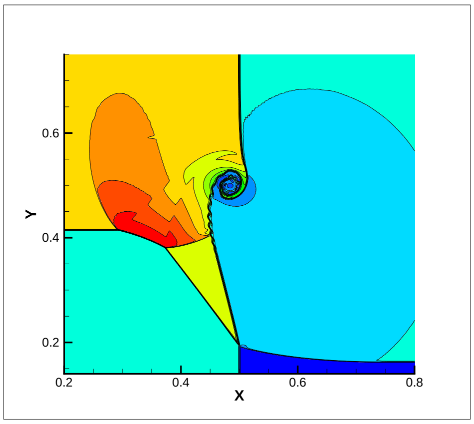

Figure 10: The density contour of WENO-PPM4.

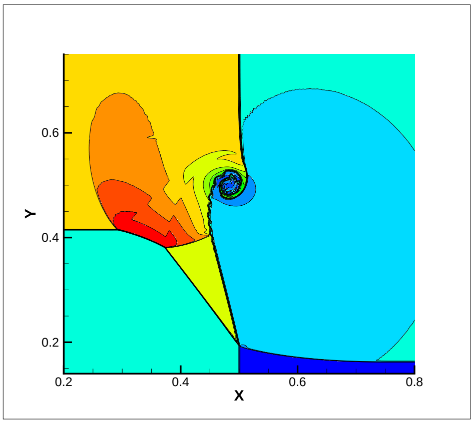

Figure 11: The density contour of WENO-PPM5.

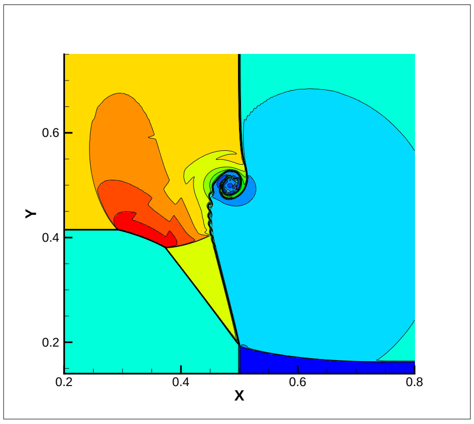

Figure 12: The density contour of WENO-PPM6.

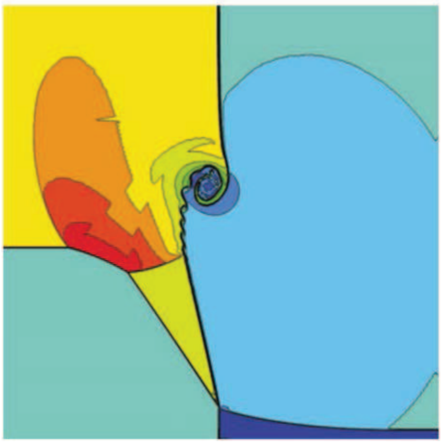

Figure 13: The density contour of WENO-7 [7].

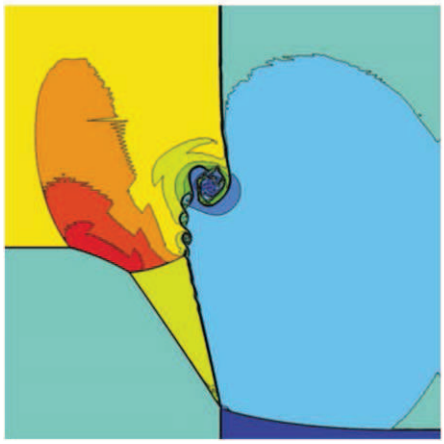

Figure 14: The density contour of the hybrid compact/WENO scheme by Pirozzoli [7].

(including WENO5 and WENO-Z) fails to resolve the instability of the slip line under current grids. Although WENO-NS has resolved the instability to some extent, its resolution is lower than WENO-PPMn schemes. The three WENO-PPMn schemes show similar performance, while WENO-PPM4 seems to give a slightly early start of the instability. WENO7, with wider stencils, also resolved the instability [7], and the unstable structures appear to have larger length scale but smaller wave numbers when compared with WENO-PPM4 and -PPM5. The hybrid compact/WENO scheme [7] gives structures with the largest length scale and the smallest wave numbers. However, obvious numerical oscillations are observed in Fig. 14, which are unfavorable for the fidelity of the result.

(3) Double-Mach reflection by a strong shock

This problem is commonly used to show the resolution of numerical schemes. As described in Ref. [2], the computational domain is chosen to be $[0,4]\times[0,1]$. The reflection wall is placed at the bottom of the domain starting from $x=1/6$. The initial condition is a right-moving Mach 10 shock positioned at $\{x=1/6,y=0\}$ at 60° to the x-axis. In order to describe the instability of the slip line generated from the triple point of the shock, a dense grid with 1920×480 cells is used. The computation runs up to $t=0.2$ with $\Delta t=0.000025$, and WENO5, WENO-M, WENO-Z, WENO-NS and WENO-PPMn are tested. Perhaps due to the small dissipation of Steger-Warming splitting, the computation of WENO-NS blew up. The density contours of WENO5, WENO-M, WENO-Z and WENO-PPM5 are shown in Fig. 15.

There are usually two concerns in this issue. One is the instability of the slip line in the region marked by dashed box in Fig. 15(a). The other is the companion structures after the primary reflection shock shown in the solid-lined box. It is evident that WENO5 cannot clearly describe the instability of the shear layer in the dashed box under such dense grids. For WENO-M, the situation is improved to some extent and some struc-

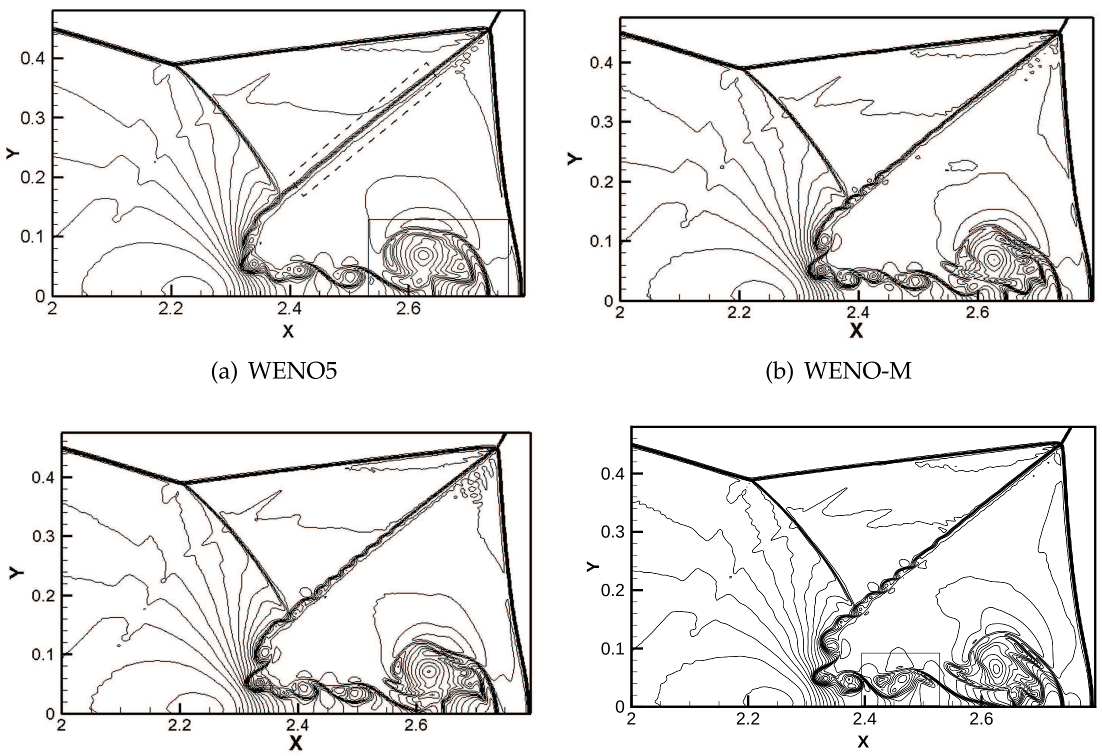

(a) WENO5

(b) WENO-M

(c) WENO-Z

(d) WENO-PPM5

Figure 15: Density contours by different schemes for double Mach reflection at $t=0.2$.

tures are captured upstream of the location where the reflection shock intersects with the slip line. WENO-Z gives an earlier occurrence of wavy structures which approximately start at $y=0.31$. The result of WENO-PPM5 is used as the representative of WENO-PPMn schemes, which shows an instability occurrence at $y=0.29\sim 0.3$. From Figs. 15, WENO-PPM5 resolves more unstable structures than WENO-M but less than WENO-Z. On the other hand, the unstable structures by WENO-PPM5 seem to be stronger and have larger oscillation amplitude than those of WENO-Z. This point is shown in Fig. 17 by the density distribution along the slip line at x-range $[2.384,2.647]$ obtained by interpolation. Regarding the companion structure, it can be seen that WENO-PPM5 gives a description with more complexities. What is more, a vortex pairing is described by WENO-PPM5, the process of which is shown in Fig. 16 and highlighted in the box in Figs. 15(d) and 16(a) and (b). On checking, such dynamics are absent in simulations of WENO-M and WENO-Z.

(4) Hypersonic flows of the sharp double cone

This case is often used to test predictions on heat flux in a shock/boundary-layer interaction. The geometry is demonstrated in the lower right inset of Fig. 18. The inflow

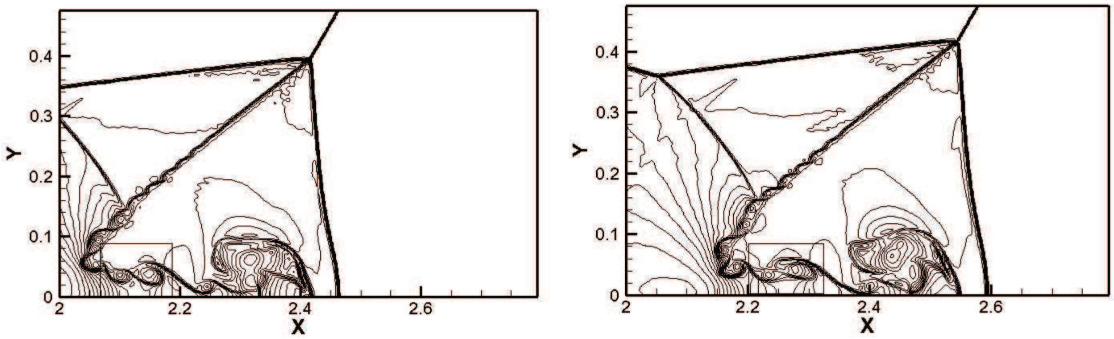

(a) $t = 0.175$ (b) $t = 0.185$

Figure 16: Density contour by WENO-PPM5 at two instances before $t = 0.2$.

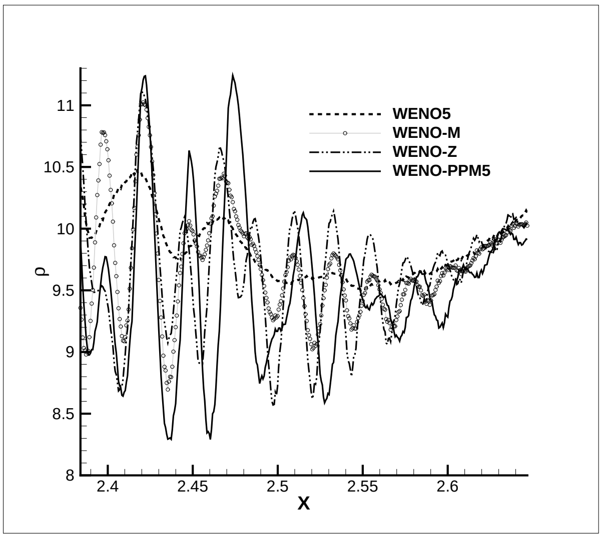

Figure 17: Comparisons of density distribution along the slip line.

conditions are: $M_\infty = 9.59$, $T_\infty = 185.6$ K, $T_w = 293.3$ K, $Re = 139436$ m^{-1}. The grid distribution is $n_{stream} \times n_{normal} = 256 \times 148$. WENO5, WENO-M and WENO-PPM5 are used in computations, while the numerical and experimental results from Gnoffo [11] are cited for reference. The grids in the computation of Ref. [11] are 512×256.

Fig. 18 shows the wave and vortex structures by WENO-PPM5. The length unit is meter. The density gradient contour indicates that a train of reflected shocks which is generated between the layer formed by the slip line and the second cone surface is resolved by the computation. In the upper inset of the figure, five vortices are resolved by the scheme, which indicates the capability of WENO-PPM5 to describe the complex hypersonic separation. Quantitative comparison of the heat flux is given in Fig. 19 by Stanton number, where all fifth-order schemes show quite similar heat flux predictions.

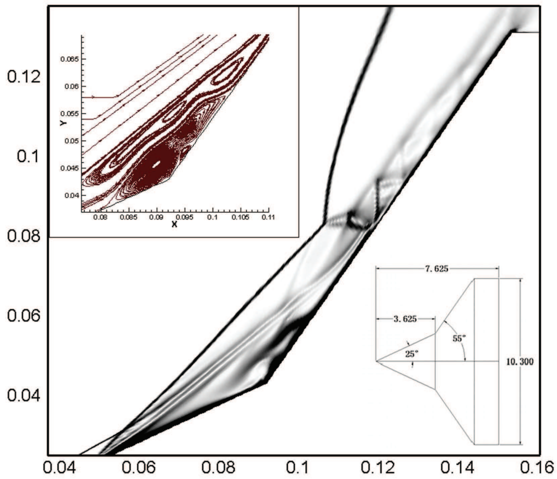

Figure 18: Contour of the magnitude of density gradient of WENO-PPM5.

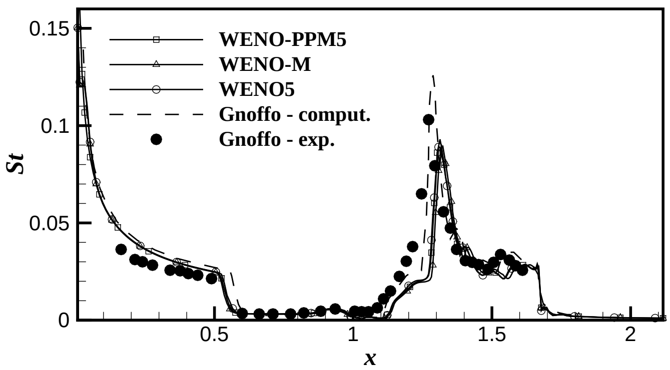

Figure 19: Heat flux of numerical predictions and experiment [11].

(5) Shock-vortex interaction

The case studied here regards a strong shock with the Mach number M_s=3 interacting with a strong vortex, which is similar to ones in Ref. [5] and [12]. The governing equations are Euler equations. A coordinate system is fixed with a shock wave for simplicity, and an isentropic vortex is superimposed ahead of the shock wave as [12]:

$$
\begin{aligned}
&u_\theta = \Gamma|\vec{r}-\vec{r}_0|/r_c e^{\left[\left(1-|\vec{r}-\vec{r}_0|^2\right)/2\right]},\\
&p(r) = \frac{1}{\gamma {M_\infty}^2}\left[1-\frac{\gamma-1}{2}\Gamma^2\exp(1-|\vec{r}-\vec{r}_0|^2)\right]^{\gamma/(\gamma-1)},\\
&\rho(r) = \left[1-\frac{\gamma-1}{2}\Gamma^2\exp(1-|\vec{r}-\vec{r}_0|^2)\right]^{1/(\gamma-1)},
\end{aligned}
$$

where u_θ denotes the tangential velocity of the vortex, $\vec{r}_0 = (4,0)$ represents the initial position of the vortex, $\gamma = 1.4$, $p(r)$ and $\rho(r)$ are initial distributions of pressure and density ahead of the shock at $x = 0$, and Γ is the vortex strength with the value 0.4. The above three relations are non-dimensionalized with the velocity u_∞, $\rho_\infty u_\infty^2$, and ρ_∞ of the inflow. The initial flow-field after the shock can be obtained by Rankine-Hugoniot relations. The computational domain is $[-20,10]\times[-15,15]$, and a uniform grid is used with the number: 1501×1501. The computation runs to $t=14$ with $\Delta t = 0.002$. Five schemes were used as: WENO5, WENO-M, WENO-Z, WENO-NS, and WENO-PPM5.

In Fig. 20, density contours of fives schemes are given, and zoomed windows are used to show a small vortex roll-up generated by the interaction. Relatively speaking, WENO5 gives the most smeared description about the roll-up, while WENO-M and WENO-Z give the moderately resolved ones. It is apparent that WENO-NS and WENO-PPM5 present richest descriptions about the roll-up structures. In addition, checks are made on the second vertical disturbing wave approximately at $x = -3.6$, which is generated by the adaption of Euler solver to initial shock wave discontinuity. It appears that the disturbing wave by WENO-NS shows features of numerical oscillations, while that by WENO-PPM5 still retains the form as that of WENO-Z and WENO-M. The result is consistent to our previous experiences that WENO-NS has less numerical stability and will be more susceptible of computation failure in cases with strong shocks.

4 Discussions

As mentioned in Section 3, it is hard for a single polynomial spanning over $[0,1]$ to efficiently fulfill five properties for all C_k of WENO5. Besides, it is natural to ask the application potential of PPM for symmetric WENO schemes. Discussions in this section relate to these aspects.

4.1 The possibility of single polynomial on $[0,1]$ as mapping function

By using Eqs. (2.12) and (2.13), a fourth-order polynomial can be uniquely determined as $b_1(a_1\omega + a_2\omega^2 + a_3\omega + a_4\omega^4)$, where $b_1 = 1/(C_k-1)^2$, $a_1 = 3-5C_k+C_k^2$, $a_2 = 3(-1+C_k+C_k^2)/C_k$, $a_3 = (1+C_k-5C_k^2)/C_k^2$ and $a_4 = (-1+2C_k)/C_k^2$. It can be shown that the polynomial will violate property (3) at $C_k = 0.1$ and property (5) at $C_k = 0.3$ as summarized in Section 2.2. Theoretically, violations can be relieved by raising the order of the polynomial and using new polynomial coefficients to fulfill the properties. Such practices are introduced subsequently according to C_k. The obtained polynomial is referred as SPM or SPMn (C_k), where n denotes the order.

(a) $C_k = 0.1$

In order to achieve monotonicity (property (3)) and have a "nice" appearance (property (5)), our practices show that the order of the polynomial should start from eleven. Regarding the polynomial derivation, Eq. (2.21) at $\omega = 1$ should be used for $i = 1,\cdots,8$

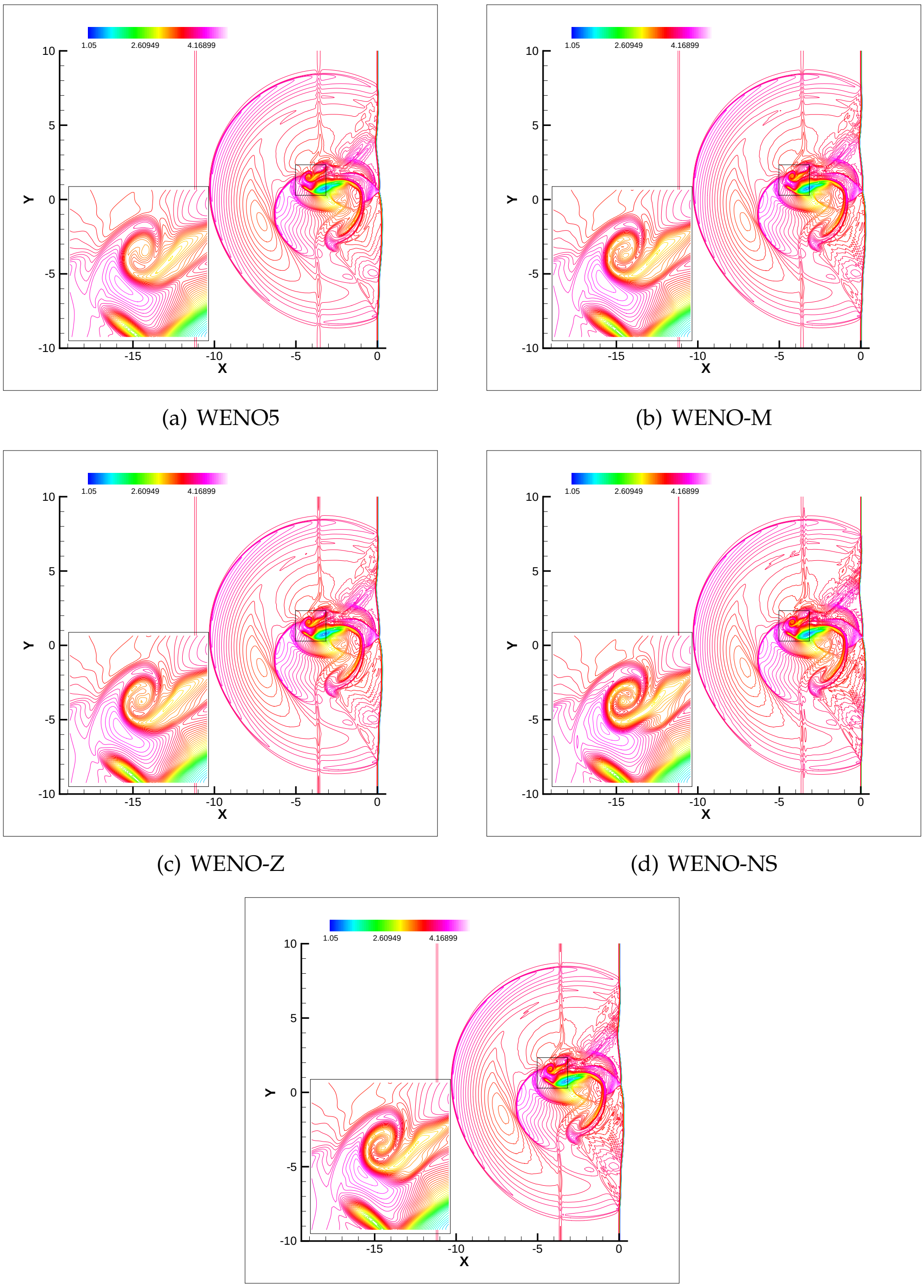

(a) WENO5

(b) WENO-M

(c) WENO-Z

(d) WENO-NS

(e) WENO-PPMS

Figure 20: Density contours of shock-vortex interaction by different scheme at $t=14$.

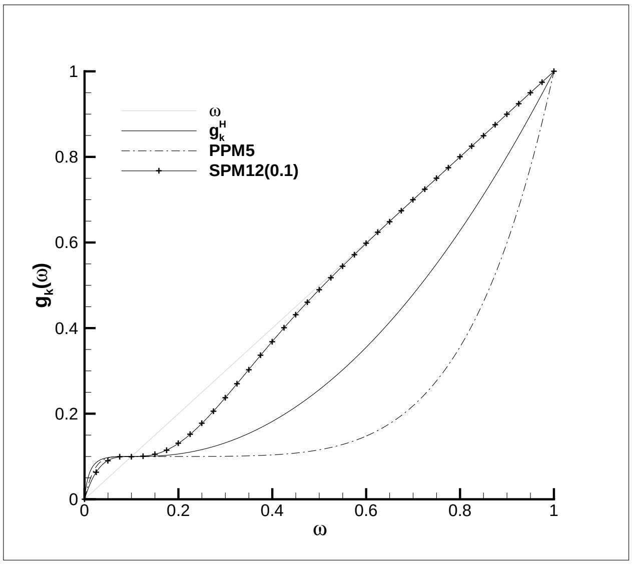

Figure 21: Mapping functions for $C_k=0.1$.

besides Eqs. (2.12) and (2.13). The number of equations can specify a twelfth-order polynomial but the outcome turns out to an eleventh-order one, which is shown in Fig. 21. From the figure, the function falls within the region enclosed by $gk(\omega)=\omega$ and g_k^H, and shows a fast convergence towards $gk(\omega)=\omega$ at $[C_k,1]$.

(b) $C_k=0.3$

For this situation, the fifth-order polynomial is found to be able to achieve properties (3) and (5), and its derivation is by using Eqs. (2.12) and (2.13) plus Eq. (2.21) at $\omega=1$ for $i=1$. The corresponding SPM5(0.3) is shown in Fig. 22. From the figure, the polynomial is inferior to g_k^H and PPM5 in the sense of property (4).

As an experiment, a polynomial with twelfth-order is tested to see if property (4) could be improved by appealing to Eq. (2.22). From trial and error, SPM12(0.3) with the preservation of monotonicity is obtained by imposing Eqs. (2.12), (2.13) and (2.21) at $\omega=0$ and 1 for $i=1$, Eq. (2.21) at $\omega=1$ for $i=2,\cdots,4$, and Eq. (2.22) for $i=3,\cdots,5$. The distribution of SPM12(0.3) is also shown in Fig. 22. Despite the obvious increase of computation due to the extra higher-order terms, the polynomial is still less flat than PPM5 at $\omega=C_k$.

(c) $C_k=0.6$

For this situation, SPM4(C_k) is found to be monotone and have a "nice" appearance. From Fig. 23, the function resembles g_k^H. Similarly, in pursuit of better performance on property (4), a twelfth-order SPW12(0.6) is derived by satisfying Eq. (2.21) at $\omega=0$ for $i=1$ and Eq. (2.22) for $i=3,\cdots,9$. The distribution of the function is also shown in Fig. 23. The figure shows that SPW12(0.6) has largely increased the flatness of the function at C_k (even a bit flatter than PPM5), which implies the potential of resolution enhancement. Nevertheless, the improvement is accomplished with the increase of computation.

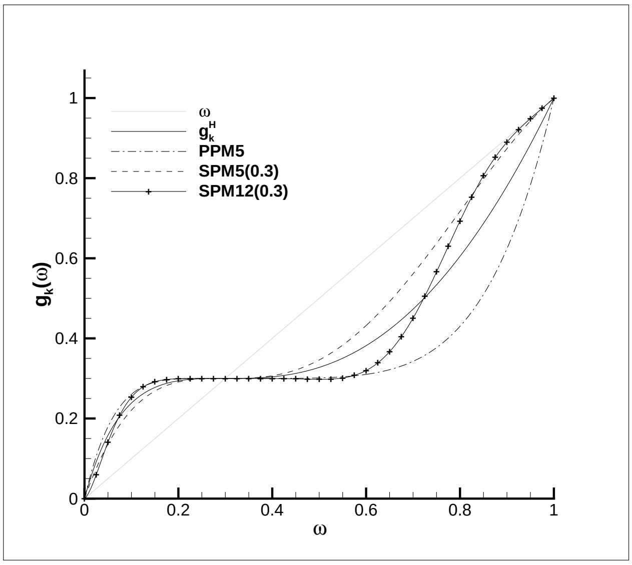

Figure 22: Mapping functions for $C_k = 0.3$.

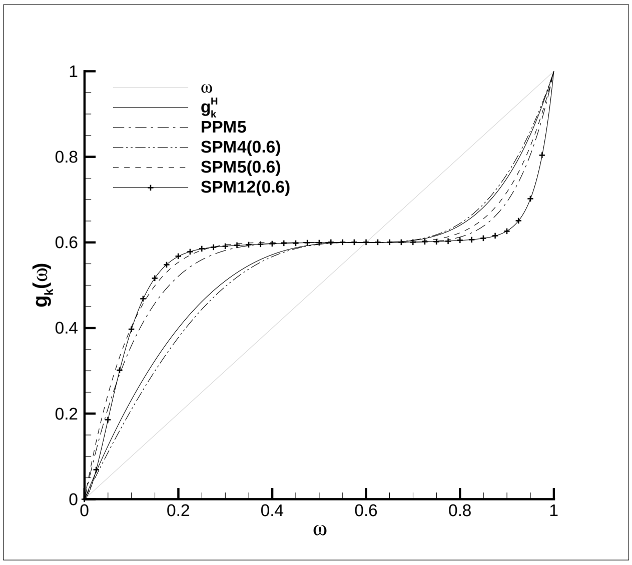

Figure 23: Mapping functions for $C_k = 0.6$.

Among polynomials with order higher than four, a fifth-order polynomial is found to be unexpectedly flatter at $\omega = C_k$ than several polynomials with higher order such as 6 and 7. The function is first derived by $g_k^{(3)}(C_k) = 0$ besides Eqs. (2.12) and (2.13). Careful checking shows the function is slightly non-monotone prior to $\omega = C_k$. This flaw can be overcome by letting $g_k^{(3)}(C_k)$ have a certain non-zero value so that the first derivative of the polynomial can only be zero at C_k. The value is solved as $9175/564-(25/188)\times 7905^{0.5}$ and the corresponding function is SPM5(0.6) shown in Fig. 23. From the figure, SPM5(0.6) does not show a distinctly flatter profile than that of PPM5.

In summary, the investigation on a single polynomial on [0,1] to serve as a mapping function proves that the fifth-order SPM cannot satisfy the property (3) and (5) at all C_k; although the twelfth-order SPM can satisfy all the properties, it still does not have a flatter profile at all C_k than that of PPM5, while its computational cost is definitely increased. So it is preferred to using PPM5 as the mapping function other than SPM.

4.2 The application potential of PPM5 for symmetric WENO5 scheme

It is known that the fifth-order symmetric WENO scheme (SWENO5) can have adjustable dissipation [8]. Thus, it is necessary to check if the PPMn functions could be used for SWENO5. The formulation of SWENO5 can be described using Eq. (2.3) by $r'=r$. Under the framework of WENO, nonlinear weights are still defined by Eq. (2.4) except their linear counterparts are: $C_k|_{k=0,\cdots,4}=(-C_3+1/10,-3C_3+3/5,3C_3+3/10,C_3)$; smoothness indicators are still described by Eq. (2.9) with the addition of $IS_3^{JS}=(13/12)(f_{j+1}-2f_{j+2}+f_{j+3})^2+(1/4)(5f_{j+1}-8f_{j+2}+3f_{j+3})^2$ [2]. In SWENO5, C_3 is a free parameter which causes the linear scheme to have varying dissipation. For example, when $C_3=0$, the linear scheme is the linear WENO5, and when $C_3=1/20$, a sixth-order central scheme results. Following the same idea of WENO-M, the symmetric version of WENO-M and WENO-PPMn can be obtained, which are referred as SWENO-M and SWENO-PPMn respectively.

Prior to the implementation of SWENO5, SWENO-M and SWENO-PPM, C_3 should be specified first. Experiences have shown that appropriate numerical dissipation is a necessity for numerical stability. The relationship of C_3 with the dissipation of SWENO5 is that the dissipation of the scheme at the scaled wave number π is $-\frac{16}{15}(1-20C_3)$ [8]. Empirically, selected numerical cases can be used to specify the largest allowable value of C_3 by checking if it can make computations essentially stable. The case used in this study is the supersonic shock/boundary layer interaction [10], which was usually used for validations. The free stream condition of the problem is: $M_\infty=2$, $T_\infty=293K$, $Re_\infty=2.96\times 10^5$, and the wall is adiabatic. The physical domain is: $0\le x\le 2.02$ and $0\le y\le 1.3$. An incident shock is introduced at the upper left corner at the angle 32.585°, which results in reflection and interaction afterwards. In addition, a separation bubble is generated at the interaction zone. By checking applicable values from 0 to 1/20 with an increment of 1/320, the largest C_3 for SWENO5 is found as 1/64, beyond which the predicted pressure coefficient oscillates. After C_3 is specified, SWENO-M and SWENO-PPM5 are tested. The computations show that both pressure distributions and separation bubbles have oscillations. The former is shown in Fig. 24 and the latter in Fig. 25 where results of SWENO-PPM5 are shown as representatives. In the figures, results of SWENO5 are utilized for comparison. Considering that SWENO-M and SWENO-PPM5 will become WENO5 when $C_3=0$, non-oscillatory results should be available if C_3 is small enough. But for the current choice of

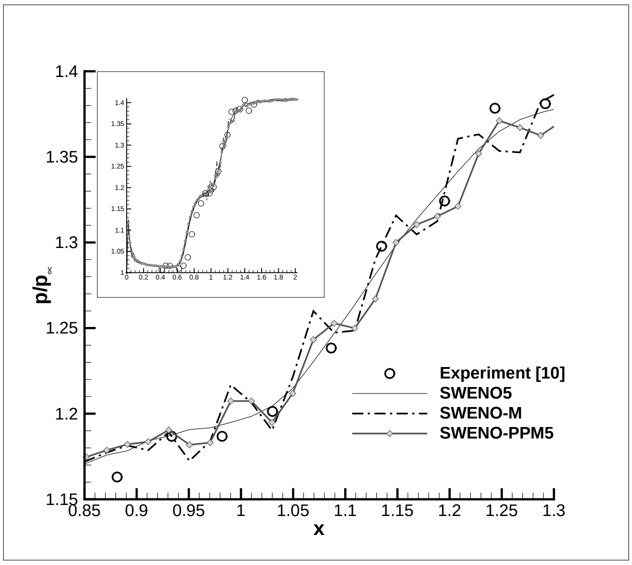

Figure 24: Pressure distribution using different schemes.

$C_3 = 1/64$, the basis of two former schemes, i.e., SWENO5, quite resembles WENO5. Numerical tests have shown the difference by further decreasing C_3 is not obvious. On the other hand, the implementation of symmetric WENO leads to an obvious computation increase. Therefore, it is not suggested to use SWENO-PPM5 other than WENO-PPM5.

5 Conclusions

The mapping function method [3] was investigated for the purpose of resolution enhancement with the preservation of numerical stability. An idea of piecewise polynomial mapping function is introduced to derive new mapping functions. The advantage of the idea is that the polynomial functions can be designed to have a controllable and more flat profile at the location of C_k than that of Henrick et al. [3], and such property is numerically favorable for resolution enhancement. Three polynomial functions are constructed thereby and corresponding schemes are referred as WENO-PPM4, -PPM5 and WENO-PPM6. 1-D and 2-D examples are tested with the comparison with WENO-M, WENO-Z and WENO-NS. Although the performance of WENO-PPMn is not prominent in the 1-D Shu-Osher problem, they perform better in 2-D Riemann and the double Mach reflection problems and show good resolution capability. Specifically, only WENO-PPMn schemes resolve the vortex-pairing phenomenon.

The reason of not suggesting single polynomials as mapping functions is also discussed. Single polynomial functions are found to be insufficient to satisfy the properties in Section 2.2 than PPM5. On the other hand, the attempt in using PPM5 for symmetric WENO shows that if SWENO-PPM5 does not sufficiently resemble WENO5 (or if C_3 is

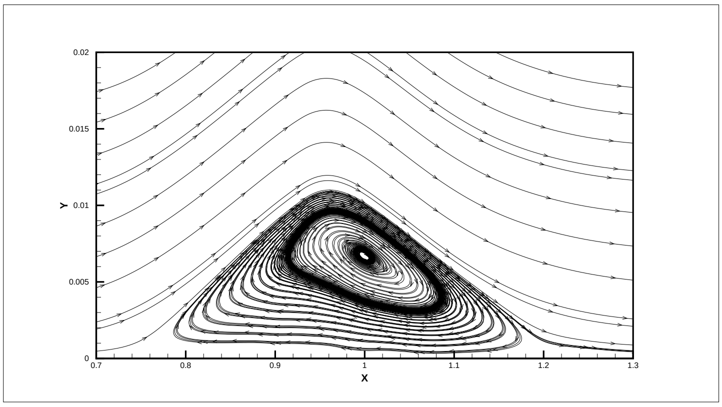

(a) SWENO5

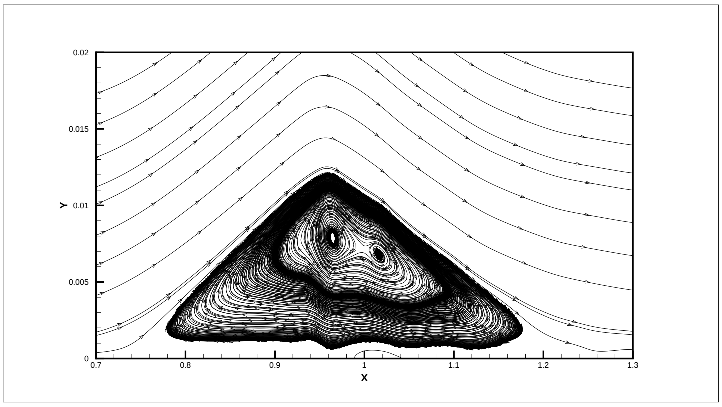

(b) SWENO5-PPM5

Figure 25: The instantaneous streamlines of different schemes with $C_3 = 1/64$.

not small enough), the result will show numerical oscillations. Therefore, PPM5 is not suggested for SWENO5.

Although WENO-PPMn schemes have overall similar performance, WENO-PPM5 appears to have the flattest profile at C_k, which is theoretically more favorable of resolution enhancement. Therefore WENO-PPM5 is tentatively suggested for applications. Additionally, it can be seen that PPM5 satisfy the accuracy requirement of WENO7 [2] and theoretically could be used for its improvement. On the other hand, PPM5 may also be used for WENO3 and SWEMO3 for potential improvement.

Acknowledgments

This work was sponsored by the National Science Foundation of China under the Grant number 91016001 and 11272037, and also partially supported by National Key Basic Research and Development 973 Program of China under Grant Number 2014CB744100. The first author is grateful to Prof. Frank Lu for his efforts on revising the manuscript.

References

[1] X.-D. Liu, S. Osher, T. Chan, Weighted essentially non-oscillatory schemes, J. Comput. Phys., 115 (1994) 200-212.
[2] G. S. Jiang, C.-W. Shu, Efficient implementation of weighted ENO schemes, J. Comput. Phys., 126 (1996) 202-228.
[3] A. K. Henrick, T. D. Aslam, J. M., Powers, Mapped weigted essentially non-oscillatory schemes: achieving optimal order near critical points, J. Comput. Phys., 207 (2005) 542-567.
[4] Y. Ha, C.-H. Kim, Y.-J. Lee, J. Yoon, An improved weighted essentially non-oscillatory scheme with a new smoothness indicator, J. Comput. Phys., 232 (2013) 68-86.
[5] R. Borges, M. Carmona, B. Costa, W-S. Don, An improved weighted essentially non-oscillatory scheme for hyperbolilc conservation laws, J. Comput. Phys., 227 (2008) 3191-3211.
[6] P. D. Lax and X-D. Liu, Solution of two-dimensional Riemann problems of gas dynamics by positive schemes, SIAM J. Sci. Comput., Vol. 19, No. 2 (1998) 319-340.
[7] S. Pirozzoli, Numerical methods for high-speed flows, Annu. Rev. Fluid Mech., 43 (2010) 163-194.
[8] Q. Li, Q.-L. Guo, H.-X. Zhang, Analyses on the dispersion overshoot and inverse dissipation of high order schemes, Adv. Appl. Math. Mech., 5 (2013) 809-824.
[9] M. P. Martn, E. M. Taylor, M. Wu, V. G. Weirs, A Bandwidth-Optimized WENO Scheme for the Direct Numerical Simulation of Compressible Turbulence, J. Comput. Phys., 220 (2006) 270-289.
[10] R. W. MacCormack, A numerical method for solving the equations of compressible viscous flow, AIAA J., 20 (1982).
[11] P. Gnoffo, CFD validation studies for hypersonic flow prediction, AIAA paper 2001-1025 (2001).
[12] O. Inoue and Y. Hattori, Sound generation by shock-vortex interactions, J. Fluid Mech., 380 (1999) 81-116.